Inorganic Chemistry

ARTICLE

pubs.acs.org/IC

Synthesis, Structure, and Thermally Stable Luminescence of Eu^{2+}-Doped $Ba_2Ln(BO_3)_2Cl$ (Ln = Y, Gd and Lu) Host Compounds

Zhiguo Xia,*[,†] Xiaoming Wang,[‡] Yingxia Wang,[‡] Libing Liao,[†] and Xiping Jing[‡]

[†]School of Materials Sciences and Technology, China University of Geosciences, Beijing 100083, P. R. China

[‡]The State Key Laboratory of Rare Earth Materials Chemistry and Applications, College of Chemistry and Molecular Engineering, Peking University, Beijing 100871, P. R. China

Supporting Information

ABSTRACT:

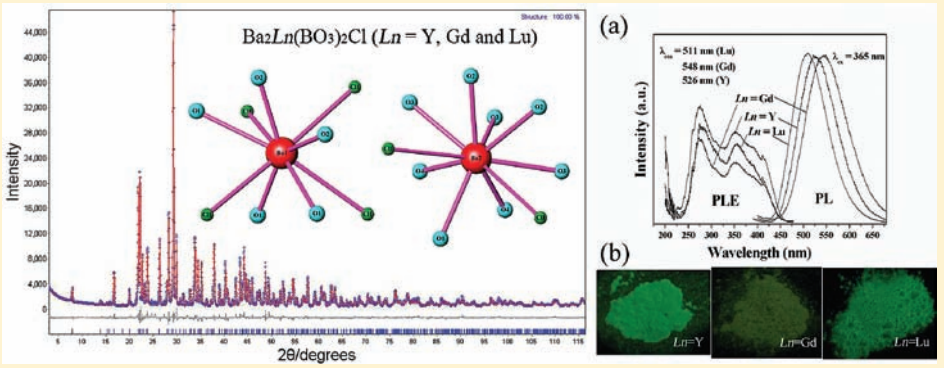

A new family of chloroborate compounds, which was investigated from the viewpoint of rare earth ion activated phosphor materials, have been synthesized by a conventional high temperature solid-state reaction. The crystal structure and thermally stable luminescence of chloroborate phosphors $Ba_2Ln(BO_3)_2Cl:Eu^{2+}$ (Ln = Y, Gd, and Lu) have been reported in this paper. X-ray diffraction studies verify the successful isomorphic substitution for Ln^{3+} sites in $Ba_2Ln(BO_3)_2Cl$ by other smaller trivalent rare earth ions, such as Sm, Eu, Tb, Dy, Ho, Er, Tm, and Yb. The detailed structure information for $Ba_2Ln(BO_3)_2Cl$ (Ln = Y, Gd, and Lu) by Rietveld analysis reveals that they all crystallize in a monoclinic $P2_1/m$ space group. These compounds display interesting and tunable photoluminescence (PL) properties after Eu^{2+}-doping. $Ba_2Ln(BO_3)_2Cl:Eu^{2+}$ phosphors exhibit bluish-green/greenish-yellow light with peak wavelengths at 526, 548, and 511 nm under 365 UV light excitation for $Ba_2Y(BO_3)_2Cl:Eu^{2+}$, $Ba_2Gd(BO_3)_2Cl:Eu^{2+}$, and $Ba_2Lu(BO_3)_2Cl:Eu^{2+}$, respectively. Furthermore, they possess a high thermal quenching temperature. With the increase of temperature, the emission bands show blue shifts with broadening bandwidths and slightly decreasing emission intensities. It is expected that this series of chloroborate phosphors can be used in white-light UV-LEDs as a good wavelength-conversion phosphor.

1. INTRODUCTION

The introduction of the halogen ions (such as F^-, Cl^-, Br^-, and I^-) into some conventional inorganic oxide compounds has great potential for the exploration of technologically important materials with special functional properties. For example, metal oxyfluorides began with the fluoride substitution into solid-state metal oxide phases shown to decrease the synthesis and sintering temperatures and to modify the physical and chemical properties.[1] Halo-containing phosphor host compounds, such as halophosphate, haloborate, halosilicate, haloaluminate, and so on, have received remarkable attention in inorganic materials science, because these compounds possess plenty of structural types and adjustable cation coordination environments. Particularly, these compounds exhibit promising optical properties by doping of rare earth activators.[2−5] As one of the hot issues in the exploration of solid-state lighting techniques, rare earth doped halo-containing phosphors, which show excellent luminescence properties under UV or blue light irradiation, have received considerable attention over past decades due to their potential applications in solid-state lighting and displays.[2−8] Therefore, more and more attention has been paid to the development of new halo-containing phosphors which can be excited in the near-ultraviolet (n-UV) and blue light range.

Considering that the optical transitions of Eu^{2+} are dipole-allowed transitions and the absorption and emission bands of Eu^{2+} are very broad, the luminescence of many kinds of Eu^{2+} activated halo-containing phosphors usually results from the ground $4f^7 6s^2 5d^0$ level to the excited $4f^6 6s^0 5d^1$ configuration, and the emission depends strongly on the crystal field around the dopant

Received: May 24, 2011
Published: September 15, 2011

ions in the host lattice.[9,10] By exploring a suitable system to accommodate Eu^{2+} ions, some previous reports have found that multiple emission colors can be realized in some novel halo-containing material systems.[2−8] In addition, as the phosphor-conversion luminescent materials in white LEDs, phosphors are generally required to have high conversion efficiency, appropriate emission colors, as well as high chemical stability. Meanwhile, they are desired to show small thermal degradation for achieving long lifetime of LEDs, which generally work at about 120 °C. That is to say, suitable phosphor systems used in white LEDs should have good thermally stable luminescence.[11]

Recently, we have made efforts to explore novel halo-containing phosphors used in white LEDs, including the preparation of some multicolor emission phosphor systems, as well as their spectral and chemical stability modifications.[7,8,12−14] Herein, we present the synthesis, crystal structure, and luminescence properties of a new family of chloroborate phosphors $Ba_2Ln(BO_3)_2Cl:Eu^{2+}$ (Ln = Y, Gd, and Lu). We have incorporated different trivalent rare earth ions in the host lattice. Rietveld analysis reveals that the successful isomorphic substitution for Ln^{3+} sites in the $Ba_2Ln(BO_3)_2Cl$ host can be implemented only for the smaller lanthanide ions (such as Y, Sm, Eu, Gd, Tb, Dy, Ho, Er, Tm, Yb, and Lu), and they all crystallize in a monoclinic $P2_1/m$ space group. Among them, $Ba_2Ln(BO_3)_2Cl$ (Ln = Y, Gd, and Lu) compounds display interesting and tunable photoluminescence (PL) properties after Eu^{2+} doping, and they exhibit bluish-green/greenish-yellow light under 365 nm UV light excitation with peak wavelengths at 526, 548, and 511 nm for $Ba_2Y(BO_3)_2Cl:Eu^{2+}$, $Ba_2Gd(BO_3)_2Cl:Eu^{2+}$, and $Ba_2Lu(BO_3)_2Cl:Eu^{2+}$, respectively. All the as-prepared $Ba_2Ln(BO_3)_2Cl:Eu^{2+}$ (Ln = Y, Gd, and Lu) phosphors also possess a high thermal quenching temperature, which enables them to be good wavelength-conversion phosphors for use in white-LEDs.

2. Experimental Section

2.1. Sample Preparation. A series of powder samples of $Ba_2Ln(BO_3)_2Cl:0.03Eu^{2+}$ (Ln = Y, La, Ce, Pr, Nd, Sm, Eu, Gd, Tb, Dy, Ho, Er, Tm, Yb, Lu) were synthesized by the high temperature solid-state synthesis method. The starting materials, $BaCO_3$ (99.9%), Ln_2O_3 (99.99%) (except for CeO_2 (99.99%) and Tb_4O_7 (99.99%)), H_3BO_3 (99.9%), $BaCl_2 \cdot 2H_2O$ (99.9%), and Eu_2O_3 (99.99%), were mixed stoichiometrically with an excess of 5 mol % of H_3BO_3 as a flux and ground thoroughly in an agate mortar. The typical mixture for the synthesis of $Ba_2Y(BO_3)_2Cl:0.03Eu^{2+}$ consisted of 1.47 mmol $BaCO_3$, 0.5 mmol Y_2O_3, 0.5 mmol $BaCl_2 \cdot 2H_2O$, 3.15 mmol H_3BO_3, and 0.015 mmol Eu_2O_3. The mixture was fired for 3 h at 1000 °C under CO reducing atmosphere.[7]

2.2. Sample Characterization. Thermogravimetry−differential thermal analysis (TG−DTA) for the mixture (such as $BaCO_3$, Y_2O_3, H_3BO_3, $BaCl_2 \cdot 2H_2O$) used in the synthesis of $Ba_2Y(BO_3)_2Cl$ was performed on a SHIMADZU model DTG-60AH TG-DTA instrument in static air with a heat rate of 2 °C/min from room temperature to 1250 °C. Powder X-ray diffraction (XRD) data were recorded by an X-ray powder diffractometer (SHIMADZU, XRD-6000, Cu Kα radiation, 40 kV, 40 mA.). The continuous scanning rate (2θ ranging from 10° to 70°) used for phase identification was 4°(2θ)/min, and step scanning rate (2θ ranging from 3° to 115°) used for Rietveld analysis was 8 s/step with a step size of 0.02°. The diffraction patterns were analyzed with the profile refinement program TOPAS version 2.1 (Bruker AXS).[15] Room temperature PL spectra were recorded by using a Hitachi F-4500 fluorescence spectrophotometer with a photomultiplier tube operating at 400 V, and a 150-W Xe lamp was used as the excitation lamp. The room temperature decay curves were recorded on a JOBIN YVON FL3-21 spectrofluorometer, and the 370 nm pulse laser radiation was used as the excitation source. The temperature-dependent luminescence properties were measured on the same F-4500 spectrophotometer, which was combined with a self-made heating attachment and a computer-controlled electric furnace.

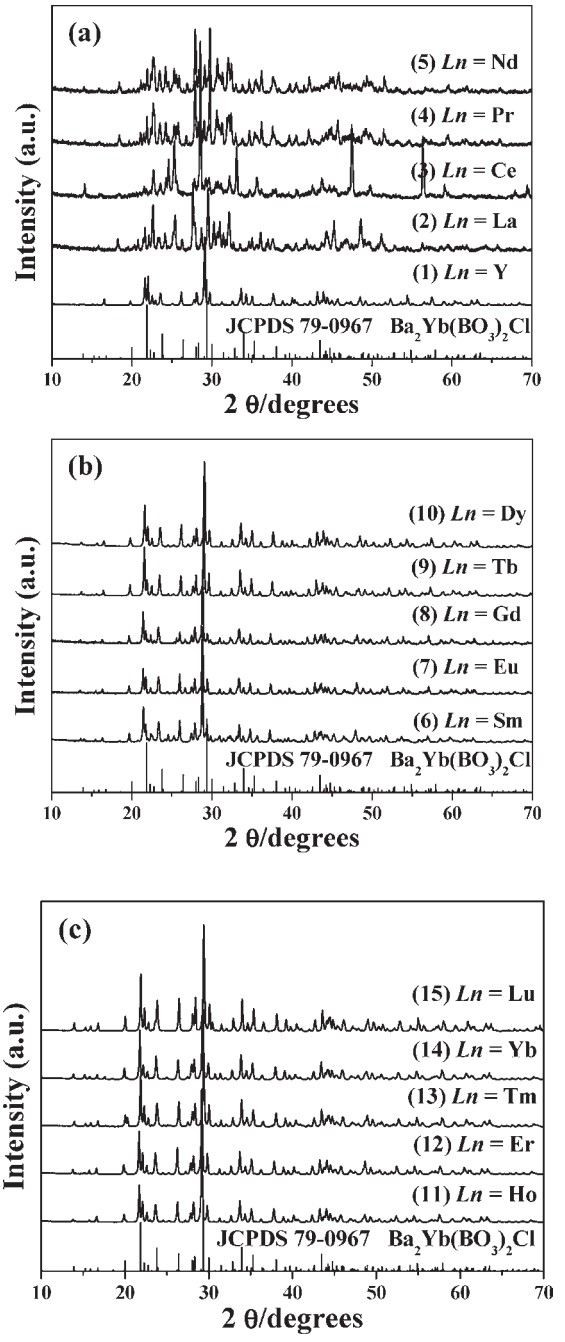

Figure 1. XRD patterns of as-prepared $Ba_2Ln(BO_3)_2Cl$ host compounds and JCPDS card (79-0967) of $Ba_2Yb(BO_3)_2Cl$: (a) (1) Ln = Y, (2) Ln = La, (3) Ln = Ce, (4) Ln = Pr, (5) Ln = Nd; (b) (6) Ln = Sm, (7) Ln = Eu, (8) Ln = Gd, (9) Ln = Tb, (10) Ln = Dy; (c) (11) Ln = Ho, (12) Ln = Er, (13) Ln = Tm, (14) Ln = Yb, (15) Ln = Lu.

3. Results and Discussion

3.1. Phase Identification and Crystal Structure. Powder X-ray diffraction profiles of $Ba_2Yb(BO_3)_2Cl$ and $Ba_2Yb(BO_3)_2Cl$

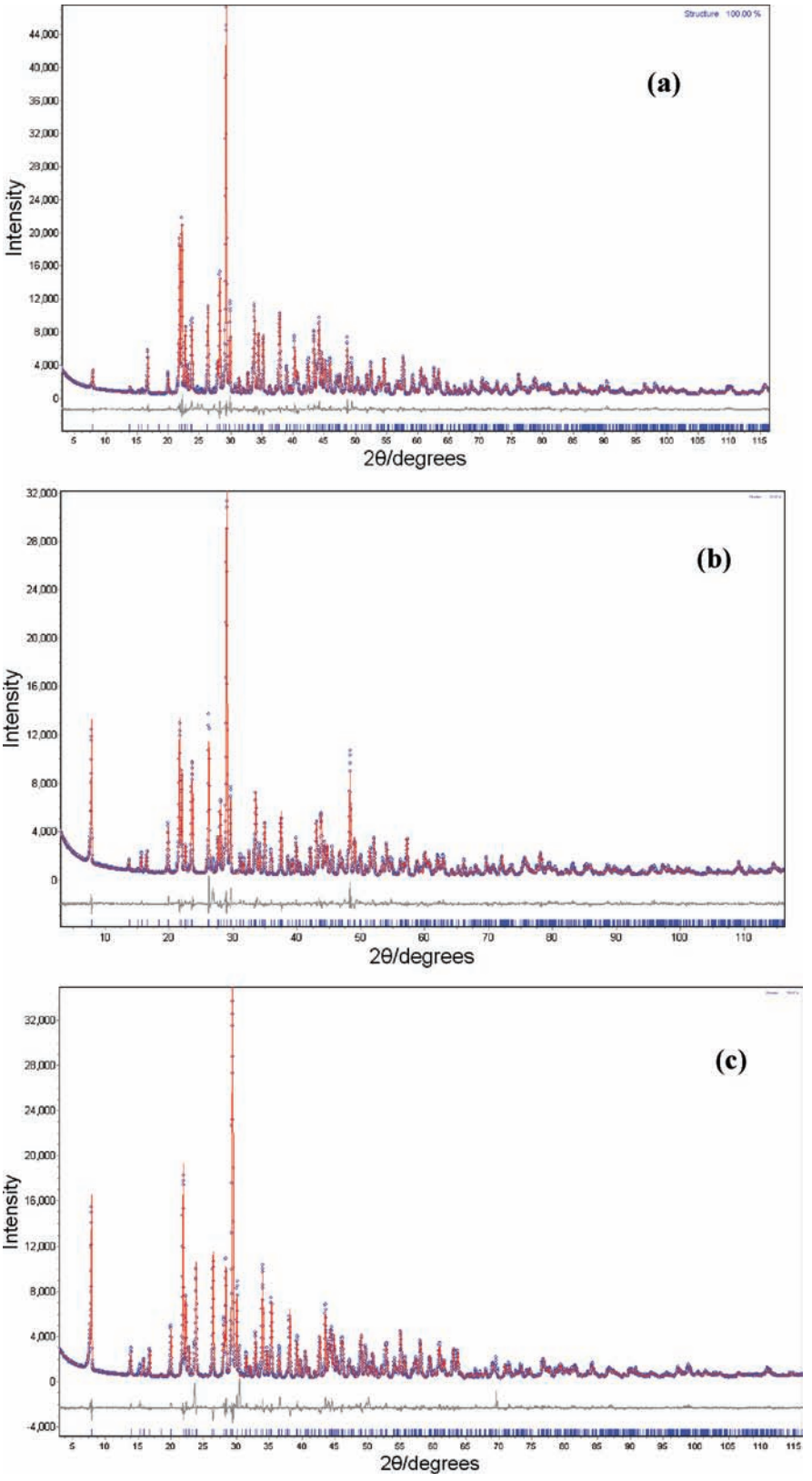

Figure 2. Rietveld analysis patterns for X-ray powder diffraction data of (a) $Ba_2Y(BO_3)_2Cl$, (b) $Ba_2GdBO_3)_2Cl$, and (c) $Ba_2Lu(BO_3)_2Cl$ samples. The solid lines are calculated intensities, and the crosses are the observed intensities. The short vertical lines show the position of Bragg reflections of the calculated pattern. The difference between the observed and calculated intensities is plotted below the profiles.

were readily identified according to the JCPDS cards 79-0967 and 79-0966, respectively. Both of them have a similar crystal structure, which crystallizes in a monoclinic unit cell with the space group $P2_1/m$. In the present study, we tried to synthesize

Table 1. Results of Structure Refinement of (a) $Ba_2Y(BO_3)_2Cl$, (b) $Ba_2Gd(BO_3)_2Cl$, and (c) $Ba_2Lu(BO_3)_2Cl$ Samples and the Comparison with $Ba_2Yb(BO_3)_2Cl$

	$Ba_2Y(BO_3)_2Cl$ (this work)	$Ba_2Gd(BO_3)_2Cl$ (this work)	$Ba_2Lu(BO_3)_2Cl$ (this work)	$Ba_2Yb(BO_3)_2Cl$ (ICSD-65934)
cryst syst	monoclinic	monoclinic	monoclinic	monoclinic
space group	$P2_1/m$	$P2_1/m$	$P2_1/m$	$P2_1/m$
V	382.41	389.83	374.95	376.77
Z	2	2	2	2
cell params	a = 6.424 Å	a = 6.467 Å	a = 6.382 Å	a = 6.397 Å
	b = 5.307 Å	b = 5.336 Å	b = 5.273 Å	b = 5.279 Å
	c = 11.279 Å	c = 11.354 Å	c = 11.206 Å	c = 11.222 Å
	β = 95.98°	β = 95.77°	β = 96.16°	β = 96.17°
profile range	$5 \le 2\theta \le 120$	$5 \le 2\theta \le 120$	$5 \le 2\theta \le 120$	
GOF	2.86	2.76	2.99	
R factors	R-Bragg 2.92%	R-Bragg 2.95%	R-Bragg 2.52%	
	R_{wp} 7.52%	R_{wp} 8.06%	R_{wp} 8.67%	
	R_p 5.43%	R_p 5.61%	R_p 5.74%	
	R_{exp} 2.63%	R_{exp} 2.92%	R_{exp} 2.90%	

$Ba_2Ln(BO_3)_2Cl$ (Ln = Y, La, Ce, Pr, Nd, Sm, Eu, Gd, Tb, Dy, Ho, Er, Tm, Yb, and Lu) compounds in order to explore a new class of chloroborate phosphors. On the basis of the carefully controlled solid-state synthesis conditions' exploration, the suitable reaction temperature for the formation of these chloroborates was 1000 °C, as given in the TG-DTA curves in Figure S1 in the Supporting Information. The XRD patterns of $Ba_2Ln(BO_3)_2Cl$ compounds are shown in Figure 1. The comparison of the XRD patterns indicates that most of the 15 trivalent rare earth ions, except for La^{3+}, Ce^{3+}, Pr^{3+}, and Nd^{3+}, can enter the framework structure of $Ba_2Ln(BO_3)_2Cl$, and the entire patterns for the other 11 kinds of barium chloride borate compounds could be well indexed similar to that of $Ba_2Yb(BO_3)_2Cl$.[16,17] It is proposed that, owing to the well-known "lanthanide contraction" effect, La^{3+} has the largest ionic radius, which will in turn restrain the phase formation in the rigid $Ba_2Ln(BO_3)_2Cl$ cell. The same phenomena can be found in Ce^{3+}, Pr^{3+}, or Nd^{3+}-substituted $Ba_2Ln(BO_3)_2Cl$ host. As also shown in Figure 1a−c, the diffraction peaks of the other 11 kinds of $Ba_2Ln(BO_3)_2Cl$ compounds similar to that of $Ba_2Yb(BO_3)_2Cl$ shift toward the smaller 2θ diffraction direction except for Yb^{3+}- or Nd^{3+}-substituted $Ba_2Ln(BO_3)_2Cl$ compounds. It should be ascribed to the successful introduction of larger radius ions of Y^{3+}, Sm^{3+}, Eu^{3+}, Gd^{3+}, Tb^{3+}, Dy^{3+}, Ho^{3+}, Er^{3+}, Tm^{3+}, compared to that of Yb^{3+}, into the $Ba_2Ln(BO_3)_2Cl$ structure, which leads to the expansion of the lattice volume. In order to confirm the structure, Rietveld structural refinements of powder diffraction patterns for $Ba_2Ln(BO_3)_2Cl$ (*Ln* = Y, Gd, and Lu) compounds were performed, as shown in Figure 2. The structural parameters reported on $Ba_2Yb(BO_3)_2Cl$ were used as initial parameters in the Rietveld analysis. Structural refinements of the three kinds of $Ba_2Ln(BO_3)_2Cl$ (Ln = Y, Gd, and Lu) were all performed by a monoclinic space group of $P2_1/m$. The refined unit cell parameters and residual factors are summarized in Table 1. For comparison, the parameters of $Ba_2Yb(BO_3)_2Cl$ are also listed in Table 1. For the $Ba_2Y(BO_3)_2Cl$ compound as an example, the residual factors are R-Bragg = 2.92%, R_{wp} = 7.52%, and R_p = 5.43% (Table 1). The unit cell parameters obtained for $Ba_2Y(BO_3)_2Cl$ are a = 6.424 Å, b = 5.307 Å, c = 11.279 Å, and β = 95.98 °, which are larger than those for $Ba_2Yb(BO_3)_2Cl$. The larger cell parameters are attributed to the larger-sized Y atoms as compared with the Yb atoms.

Considering that $Ba_2Ln(BO_3)_2Cl$ (Ln = Y, Gd, and Lu) compounds have the similar crystal structure type, the crystal structure description for the three kinds of typical $Ba_2Ln(BO_3)_2Cl$ (Ln = Y, Gd, and Lu) can be given by the same framework diagram. Figure 3 shows the projections of the structures of the $Ba_2Ln(BO_3)_2Cl$ (Ln = Y, Gd, and Lu) along different directions. All the bond distances and angles are in the normal range, and the detailed information is given in the Supporting Information. As given in Figure 3, the purple part in the packing diagram represents the Ba1 polyhedron, the red one represents the Ba2 polyhedron, and the blue one represents the LnO_7 polyhedron. The structure unit of $Ba_2Ln(BO_3)_2Cl$ (Ln = Y, Gd, and Lu) is constructed by isolated BO_3 triangles and (Ba−O, Cl) and (Ln−O) polyhedra, which is similar to the crystal structures of homologous compounds $Ba_2Ln(BO_3)_2Cl$ (Ln = Ho, Yb). However, the bond distances of Ba−O and Ba−Cl for the $Ba_2Ln(BO_3)_2Cl$ (Ln = Y, Gd and Lu) compounds in the present work are in the ranges 255.0(9)−302.3(2) and 315.8(4)−319.7(8) pm, respectively. All values are in agreement with the typical values of Ba−O and Ba−Cl bonds ($Ba_2B_5O_9Cl \cdot 0.5H_2O$: Ba−O 262.3−307.3 pm, Ba−Cl 298.1−320.1 pm).[17] The B atoms are triangularly coordinated forming BO_3 groups which are isolated from each other. They share edges or corners with Ba polyhedra to form a three-dimensional network (see Figure 3). Figure 4 shows the ball-and-stick representations of the $Ba_2Ln(BO_3)_2Cl$ (Ln = Y, Gd, and Lu) compounds, emphasizing the coordination environments, in which two $Ba(1)O_5Cl_4$ polyhedra are connected by sharing edges on two Cl atoms and two $Ba(2)O_8Cl_2$ polyhedra are connected by sharing edges on two O atoms, respectively. It can be seen that LnO_7 polyhedra are irregular with site symmetry C_s, and all these polyhedra form the network structure by edge sharing of O and Cl atoms. Therefore, in the structure of $Ba_2Ln(BO_3)_2Cl$ (Ln = Y, Gd, and Lu), the Ba atoms occupy two different sites (Ba(1) and Ba(2)), and they have a complex coordination: Ba(1) is 9-fold coordinated by 5O and 4C1, while Ba(2) is 10-fold coordinated by 8O and 2C1, as given in Figure 5. It clearly demonstrates that two different Ba^{2+} ion

dx.doi.org/10.1021/ic200988w |*Inorg. Chem.* 2011, 50, 10134–10142

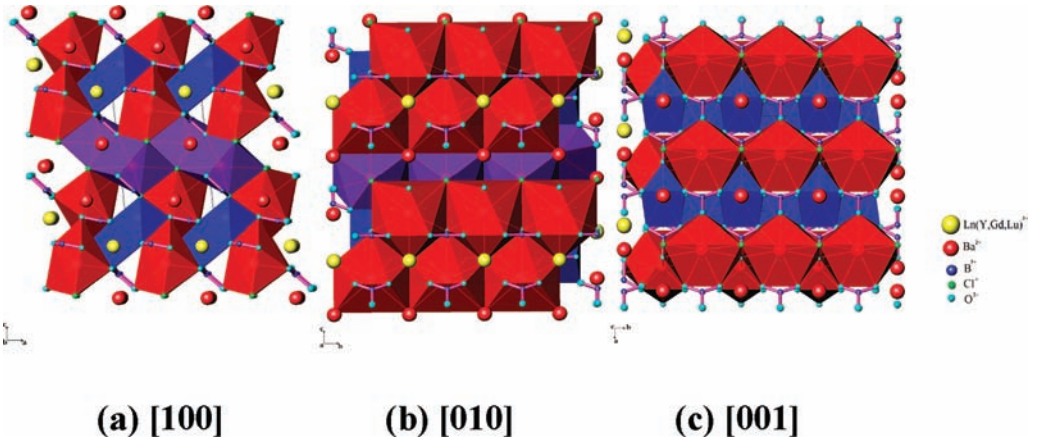

Figure 3. Proposed crystal structure model of the $Ba_2Ln(BO_3)_2Cl$ (Ln = Y, Gd, and Lu) compound: (a) view along [100], (b) view along [010], (c) view along [001]. The purple part in the packing diagram represents the Ba1 polyhedron, the red one represents the Ba2 polyhedron, and the blue one represents the LnO_7 polyhedron.

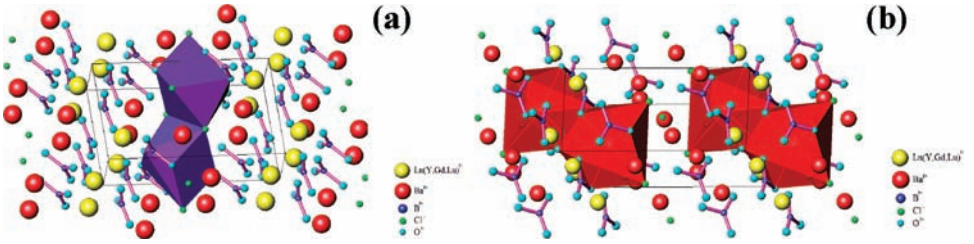

Figure 4. Ball-and-stick representations of the $Ba_2Ln(BO_3)_2Cl$ (Ln = Y, Gd, and Lu) compound emphasizing the coordination environments of (a) $Ba^1O_5Cl_4$ polyhedra by sharing edges on two Cl atoms and (b) $Ba^2O_8Cl_2$ polyhedra by sharing edges on two O atoms.

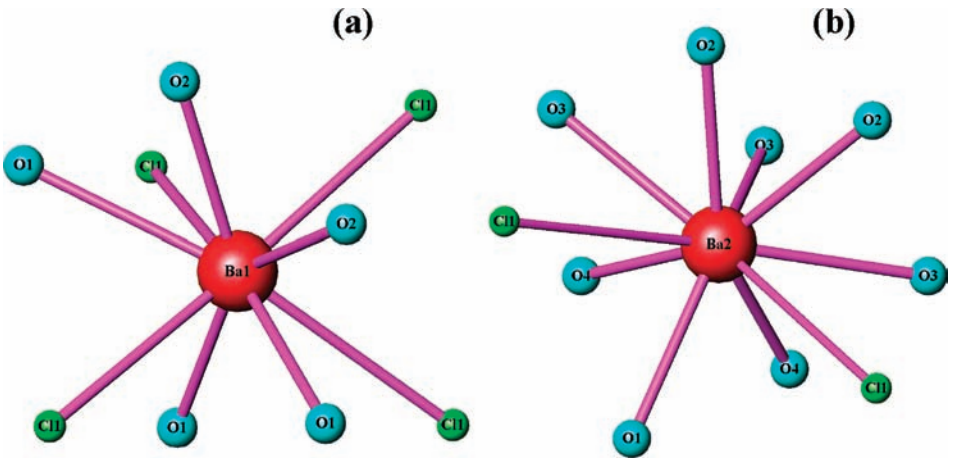

Figure 5. Coordination spheres of the two different Ba^{2+} positions in $Ba_2Ln(BO_3)_2Cl$ compound: (a) Ba(1) is 9-fold coordinated by 5O and 4C1 and (b) Ba(2) is 10-fold coordinated by 8O and 2C1.

sites Ba(1) and Ba(2) in the $Ba_2Ln(BO_3)_2Cl$ crystal structure can be occupied as the emission centers after Eu^{2+} doping.

3.2. Photoluminescence Properties of Eu^{2+} in $Ba_2Ln(BO_3)_2Cl$ (Ln = Y, Gd, and Lu). The photoluminescence excitation (PLE) and emission (PL) spectra of $Ba_2Ln(BO_3)_2Cl:0.03Eu^{2+}$ (Ln = Y, Gd, and Lu) are shown in Figure 6a. It is found that $Ba_2Ln(BO_3)_2Cl:Eu^{2+}$ phosphors exhibit bluish-green/greenish-yellow light for the naked eyes upon 365 nm UV excitation, as shown in the digital photographs (Figure 6b). The broadband emission spectra with peak wavelengths at 526, 548, and 511 nm can be found and show full width at half maximums (FWHMs) of 97, 108, and 91 nm, for $Ba_2Y(BO_3)_2Cl:Eu^{2+}$, $Ba_2Gd(BO_3)_2Cl:Eu^{2+}$, and $Ba_2Lu(BO_3)_2Cl:Eu^{2+}$ phosphors, respectively. All the broad emissions in the $Ba_2Ln(BO_3)_2Cl:Eu^{2+}$ samples are essentially assigned to the $4f^6 6s^0 5d^1 - 4f^7 6s^2 5d^0$ transition of the Eu^{2+} ion on the single cation ions site. However, two different Ba^{2+} ion

dx.doi.org/10.1021/ic200988w |*Inorg. Chem.* 2011, 50, 10134–10142

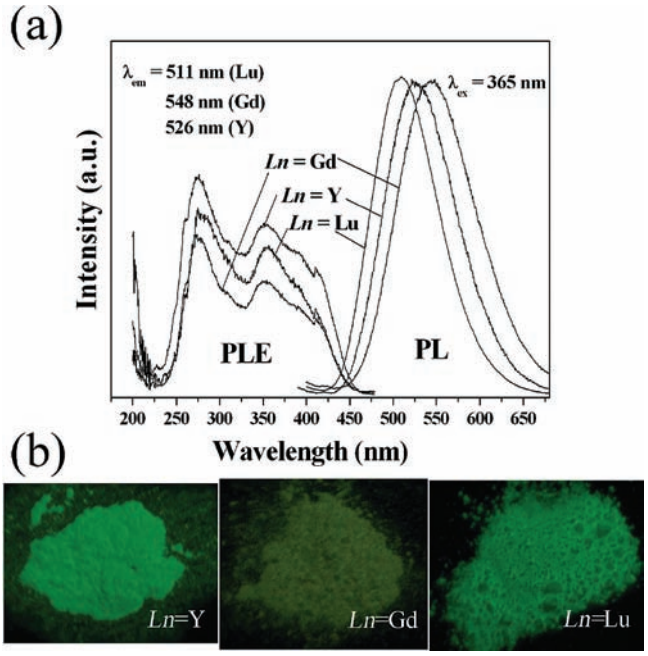

Figure 6. (a) PLE and PL spectra and (b) digital photographs under 365 nm UV light of $Ba_2Ln(BO_3)_2Cl:0.03Eu^{2+}$ (Ln = Y, Gd, and Lu) phosphors.

sites Ba(1) and Ba(2) in the $Ba_2Ln(BO_3)_2Cl$ crystal structure have been verified in the above crystal structure description. By a careful identification, we can find a very weak emission peak near 420 nm, which should correspond to the second Ba^{2+} ions sites, as also mentioned in G. Blasse's previous work.[17] It is proposed that the emission peak near 420 nm is quenched at room temperature, so that we can hardly find the obvious emission intensities.[18] In order to further understand the origin of the dominant emission band above 500 nm for three kinds of $Ba_2Ln(BO_3)_2Cl:0.03Eu^{2+}$ phosphors, the well-known experiential equation given by Van Uitert has been used to qualitatively analyze the present experimental result.[19]

According to the report of Van Uitert,[19] for Eu^{2+} in suitable matrices, the following experiential equation, eq 1, provides a good fit to the emission peak and excitation edge data. On the basis of this, the problem about which kind of crystallographic site substituted by Eu^{2+} in $Ba_2Ln(BO_3)_2Cl$ can be investigated theoretically.

$$E = Q\left[1 - \left(\frac{V}{4}\right)^{1/V} 10^{-near/80}\right] \quad (1)$$

In eq 1, E represents the position of the d-band edge in energy for rare earth ions (cm^{-1}), Q is the position in energy for the lower d-band edge for the free ions, and it is 34 000 cm^{-1} for Eu^{2+}, and V is the valence of the "active" cation, here $V = 2$. ea is the electron affinity of the atoms that form anions. n is the number of anions in the immediate shell about this ion, and r is the radius of the host cation replaced by the "active" cation. Considering that the ea value in the present $Ba_2Ln(BO_3)_2Cl$ host is very complex, we can hardly obtain the specific value to calculate the d-band edge. However, ea value should be fixed in each of the $Ba_2Ln(BO_3)_2Cl$ hosts, and a qualitatively analysis is thus conducted as follows. According to eq 1, while Ba^{2+} is substituted by Eu^{2+}, the emission band positions shift toward the long wavelength direction if the value of coordination number n of Ba^{2+} in $Ba_2Ln(BO_3)_2Cl$ host decreases. That is to say, the observed Eu^{2+} emission above 500 nm in the $Ba_2Ln(BO_3)_2Cl$ host should come from the 9-fold coordinated Ba(1) site. In the structure of $Ba_2Ln(BO_3)_2Cl$, Ba(1) is 9-fold coordinated by 5O and 4Cl, while Ba(2) is 10-fold coordinated by 8O and 2Cl. When Eu^{2+} replaces the Ba(1) position with 9-coordination (5O, 4Cl), the broad-band emission peaks at 526, 548, and 511 nm can be observed at room temperature for $Ba_2Y(BO_3)_2Cl:Eu^{2+}$, $Ba_2Gd(BO_3)_2Cl:Eu^{2+}$, and $Ba_2Lu(BO_3)_2Cl:Eu^{2+}$ phosphors, respectively. However, the weak emission bands at or near 420 nm were ascribed to the Eu^{2+} luminescence substituted Ba(2) position with 10-coordination (8O, 2C1), and quenching behavior at room temperature may be ascribed to thermally activated energy transfer to the Eu^{2+} center with the long wavelength emission band.

As for the emission difference of Eu^{2+} among $Ba_2Ln(BO_3)_2Cl$ (Ln = Y, Gd, and Lu) host lattices, it should come from the electronic configurations properties of rare earth ions in the host. As mentioned above, the broad emissions in the $Ba_2Ln(BO_3)_2Cl:0.03Eu^{2+}$ are assigned to the $4f^6 6s^0 5d^1 - 4f^7 6s^2 5d^0$ transition of the Eu^{2+} ion. It is well-known that the 5d wave function has large spatial extension, and it depends on the surroundings of Eu^{2+} ions. Thus, the different crystal lattice environment is a critical parameter for the optical properties of the Eu^{2+} ions. In $Ba_2Ln(BO_3)_2Cl$ host, the LnO_7 polyhedra are irregular with site symmetry C_s, and the effective ion radius of 7-fold coordinated Y^{3+}, Gd^{3+}, and Lu^{3+} ions are 0.096, 0.100, and 0.090 nm, respectively. As the immediate neighbor ions around the Eu^{2+} emission centers, there are two possibilities which can cause variation among the broad-band emission peaks at 526, 548, and 511 nm for $Ba_2Y(BO_3)_2Cl:Eu^{2+}$, $Ba_2Gd(BO_3)_2Cl:Eu^{2+}$, and $Ba_2Lu(BO_3)_2Cl:Eu^{2+}$ phosphors.[9] One is that the covalent degree of chemical bonds increases with the increasing ion radius from Gd^{3+}, to Y^{3+}, to Lu^{3+} in the $Ba_2Ln(BO_3)_2Cl$ host, leading to the decrease of the energy difference between 4f and 5d energy levels. The other reason is related to the strong nephelanxetic effect, which is also supported by the observed FWHMs of 97, 108, and 91 nm for $Ba_2Y(BO_3)_2Cl:Eu^{2+}$, $Ba_2Gd(BO_3)_2Cl:Eu^{2+}$, and $Ba_2Lu(BO_3)_2Cl:Eu^{2+}$ phosphors, resulting in a decrease of the energy gravity between 4f and 5d energy levels. The above two evidence prove that the $Ba_2Gd(BO_3)_2Cl:Eu^{2+}$ should have the biggest Stokes shift, and the red-shift wavelength is 183 nm, while the $Ba_2Lu(BO_3)_2Cl:Eu^{2+}$ phosphor has the smallest one of 146 nm.

Typical excitation spectra of $Ba_2Ln(BO_3)_2Cl:0.03Eu^{2+}$ phosphors are also presented in Figure 6a. Although the three excitation spectra corresponding to $Ba_2Y(BO_3)_2Cl:Eu^{2+}$, $Ba_2Gd(BO_3)_2Cl:Eu^{2+}$, and $Ba_2Lu(BO_3)_2Cl:Eu^{2+}$ phosphors were monitored by different wavelengths of 526, 548, and 511 nm, they display the same spectra profiles showing a broad peak from 250 to 450 nm, which can be attributed to $4f^6 6s^0 5d^1 - 4f^7 6s^2 5d^0$ transition of Eu^{2+} ions. As for the monitoring peaks above 500 nm for $Ba_2Ln(BO_3)_2Cl:0.03Eu^{2+}$ phosphors, they were all ascribed to the Eu^{2+} luminescence substituted in the same crystallographic Ba(1) position with 9-coordination. The point symmetry of Ba(1) site is C_s. When the Eu^{2+} ion occupies a lattice site with C_s symmetry, a splitting into five 5d bands is expected in the excitation spectra.[19] Due to the serious overlap, only two dominating 5d bands (at about 275 and 355 nm) can be observed in the excitation spectra of $Ba_2Ln(BO_3)_2Cl:0.03Eu^{2+}$ phosphors, and both of them contain some shoulder excitation bands at the edge of the dominated peaks.

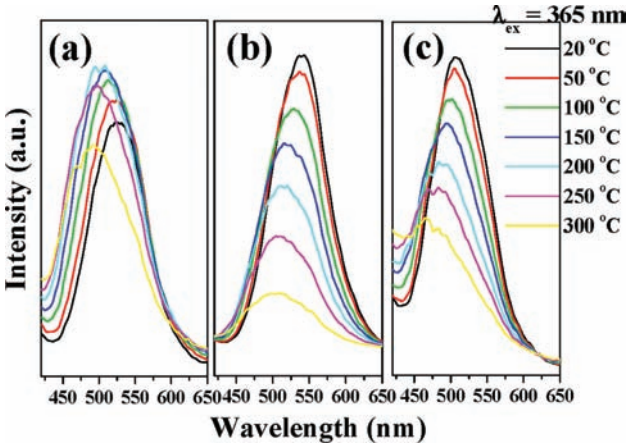

Figure 7. Emission spectra of (a) $Ba_2Y(BO_3)_2Cl$:0.03Eu^{2+}, (b) $Ba_2Gd(BO_3)_2Cl$:0.03Eu^{2+}, and (c) $Ba_2Lu(BO_3)_2Cl$:0.03Eu^{2+} phosphors at different temperatures from 20 to 300 °C under the excitation of 365 nm.

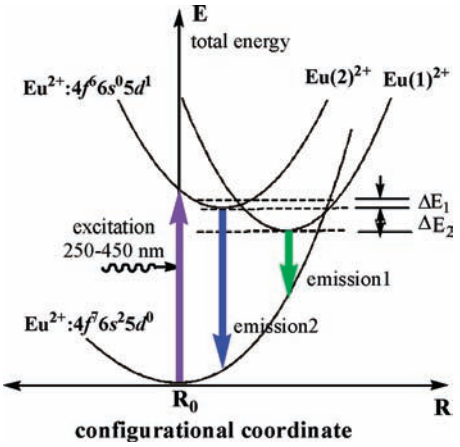

Figure 8. Schematic illustration of a configurational coordinate diagram of the ground state (Eu^{2+}: $4f^7$), two split excited states ($Eu(1)^{2+}$ and $Eu(2)^{2+}$), and ΔE_1 showing the energy barrier of the transition $Eu(2)^{2+}$ state to $Eu(1)^{2+}$, and ΔE_2 showing the energy barrier of the transition $Eu(1)^{2+}$ state to $Eu(2)^{2+}$.

The room temperature lifetimes of Eu^{2+} emissions at 526, 548, and 511 nm corresponding to $Ba_2Y(BO_3)_2Cl$:0.03Eu^{2+}, $Ba_2Gd(BO_3)_2Cl$:0.03Eu^{2+}, and $Ba_2Lu(BO_3)_2Cl$:0.03Eu^{2+} phosphors under the excitation of 355 nm were measured. The PL decay curves of the Eu^{2+} emissions and the corresponding fitting curves are presented in Figure S2. The decay curve can be well fitted with a second-order exponential decay model by the following equation:

$$I(t) = A_1 \exp(-t/t_1) + A_2 \exp(-t/t_2) \quad (2)$$

Here, I is the luminescence intensity, A_1 and A_2 are constants, t is the time, and t_1 and t_2 are the lifetimes for the exponential components. The values of t_1 and t_2 are listed in Figure S2. Further, the effective time constant (t^*) can be calculated as the following eq 3[20].

$$t^* = (A_1t_1^2 + A_2t_2^2)/(A_1t_1 + A_2t_2) \quad (3)$$

On the basis of eq 3, the decay times were determined to be 1.68, 1.40, and 1.27 μs for $Ba_2Y(BO_3)_2Cl$:0.03Eu^{2+}, $Ba_2Gd(BO_3)_2Cl$:0.03Eu^{2+}, and $Ba_2Lu(BO_3)_2Cl$:0.03Eu^{2+} phosphors, respectively. Considering that Eu^{2+} located in this series of $Ba_2Ln(BO_3)_2Cl$ compounds should have a similar chemical environment, the measured decay time is nearly the same, and the fluorescence lifetime results also show that they are short enough for potential applications in solid-state lighting.[21]

3.3. Thermally Stable Luminescence of Eu^{2+} in $Ba_2Ln(BO_3)_2Cl$ (Ln = Y, Gd ,and Lu). The thermal quenching property is one of the important technological parameters for phosphors used in solid-state lighting because it has considerable influence on the light output and color rendering index. The temperature dependence of the PL emission spectra of $Ba_2Y(BO_3)_2Cl$:0.03Eu^{2+}, $Ba_2Gd(BO_3)_2Cl$:0.03Eu^{2+}, and $Ba_2Lu(BO_3)_2Cl$:0.03Eu^{2+} phosphors excited by 365-nm UV light are illustrated in Figure 7. It shows that this series of $Ba_2Ln(BO_3)_2Cl$:0.03Eu^{2+} phosphors have excellent thermal stability. Especially, upon heating the phosphor samples in a temperature range from 20 to 200 °C, an abnormal increase of the emission intensity is apparent for the $Ba_2Y(BO_3)_2Cl$:0.03Eu^{2+} phosphor. This interesting phenomenon will be discussed below. For the $Ba_2Gd(BO_3)_2Cl$:0.03Eu^{2+} and $Ba_2Lu(BO_3)_2Cl$:0.03Eu^{2+} phosphors, the emission intensities decrease gradually. Additionally, an obvious blue shift above 30 nm is observed from 20 to 200 °C for the three kinds of $Ba_2Ln(BO_3)_2Cl$:0.03Eu^{2+} phosphors. In most cases, the peak positions of emission spectra are red-shifted with increasing temperature, and the red-shift behavior can be explained by the Varshini equation for temperature dependence[22,23]

$$E(T) = E_0 - \frac{aT^2}{T + b} \quad (4)$$

where $E(T)$ is the energy difference between excited states and ground states at a temperature T, E_0 is the energy difference at 0 K, and a and b are fitting parameters. At a high temperature, the bond lengths between the luminescent center (e.g., Eu^{2+}) and its ligand ions increase, resulting in the decreased crystal field. Therefore, it will cause the split of degenerate excited state or ground state, which results in the decrease of the transition energy. So the emission peak is red-shifted with the increase of temperature.[22] However, the emission spectra in this series of $Ba_2Ln(BO_3)_2Cl$:0.03Eu^{2+} phosphors are blue-shifted with increasing temperature. The temperature-induced blue-shift cannot be described by eq 4. This blue shift can be explained in terms of the thermally active phonon assisted excitation from a lower energy sublevel to a high energy sublevel in the excited state of Eu^{2+}.[22−24] It is proved that there should be two different Eu^{2+} ion sites in the $Ba_2Ln(BO_3)_2Cl$ crystal structure. Figure 8 shows the schematic illustration of a configurational coordinate diagram of the ground state (Eu^{2+}: $4f^76s^25d^0$) and two split excited states ($Eu(1)^{2+}$ and $Eu(2)^{2+}$) in the present phosphor system. Since $Eu(1)^{2+}$ and $Eu(2)^{2+}$ ions experience different crystal field strengths, the $4f^66s^05d^1$ excited states are located at different energy levels. The excitation state transformed to the ground state with different energy values when they were excited by the near UV light from 250 to 450 nm.[22] For the two emission centers, the barrier ΔE_1 can be overcome and the low-energy emission ($Eu(1)$) is dominant at low temperatures. At a high temperature, the thermal back-transfer over the barrier ΔE_2 is possible, and consequently the high energy emission ($Eu(2)$) is dominant. Thus, the blue-shift behavior is observed. This mechanism has been proposed in the discussion of the temperature dependent spectra of Ca_2SiO_4:Eu^{2+},[23] and further supported to be valid for $NaCaPO_4$:Eu^{2+}.[24] Therefore, the blue-shift behavior should be common in these

dx.doi.org/10.1021/ic200988w |Inorg. Chem. 2011, 50, 10134–10142

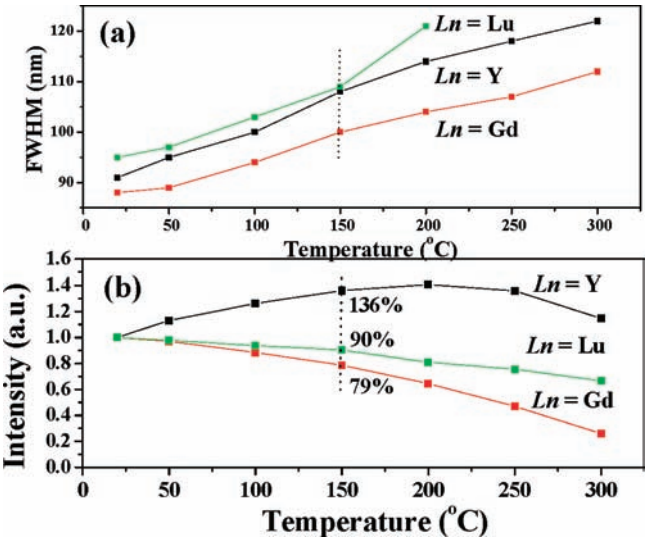

Figure 9. Temperature dependence of the FWHMs of the (a) emissions and (b) integrated emission intensities of $Ba_2Ln(BO_3)_2Cl:0.03Eu^{2+}$ (Ln = Y, Gd, and Lu) phosphors.

silicates, phosphates, and the present chloroborate phosphors considering that there are the same multisite structures for Eu^{2+} ions.

In order to further illustrate the variation of the temperature dependent emission spectra for the $Ba_2Ln(BO_3)_2Cl:0.03Eu^{2+}$ phosphors, Figure 9 shows the temperature dependence of the FWHMs of the (a) emissions and (b) integrated emission intensities of $Ba_2Y(BO_3)_2Cl:0.03Eu^{2+}$, $Ba_2Gd(BO_3)_2Cl:0.03Eu^{2+}$, and $Ba_2Lu(BO_3)_2Cl:0.03Eu^{2+}$ phosphors. In Figure 9a, the FWHM of this series of $Ba_2Ln(BO_3)_2Cl:0.03Eu^{2+}$ phosphors' emission increases gradually with increasing temperature. It is well-known that the thermally activated luminescent center is strongly interacting with a thermally active phonon, contributing to the variation of the FWHM of emission spectrum.[25] At a high temperature, the population density of phonon increases, and the electron–phonon interaction is dominant, and consequently the FWHM of emission spectrum is broadened. Furthermore, the nonraditive transition probability by thermal activation is also strongly dependent on temperature resulting in the decrease of emission intensity. However, the present $Ba_2Y(BO_3)_2Cl:0.03Eu^{2+}$ phosphor is not such a case. As given in Figure 9b, it represents the temperature dependence of the integrated emission intensity normalized with respect to the value at room temperature. It can be clearly seen that the $Ba_2Ln(BO_3)_2Cl:0.03Eu^{2+}$ phosphors have a comparatively good temperature quenching effect. When the temperature increases up to 150 °C, the normalized emission intensity is found to be 136%, 90%, and 79% of the initial value for $Ba_2Y(BO_3)_2Cl:Eu^{2+}$, $Ba_2Gd(BO_3)_2Cl:Eu^{2+}$, and $Ba_2Lu(BO_3)_2Cl:Eu^{2+}$, respectively. Especially, the as-prepared $Ba_2Y(BO_3)_2Cl:0.03Eu^{2+}$ phosphor has the abnormal temperature dependent emission property. Emission intensity of $Ba_2Y(BO_3)_2Cl:Eu^{2+}$ increases from room temperature to 200 °C, and then it decreases slightly. The emission spectra variation of $Ba_2Y(BO_3)_2Cl:0.03Eu^{2+}$ from room temperature to 300 °C, and then to 100 °C, is also given in Figure S3. It is found that the temperature dependent emission spectra of $Ba_2Y(BO_3)_2Cl:0.03Eu^{2+}$ have reversible variation behavior from 300 to 100 °C compared to the increasing temperature range. Such an excellent thermal property is very attractive in our present work. We proposed that the reason should be related

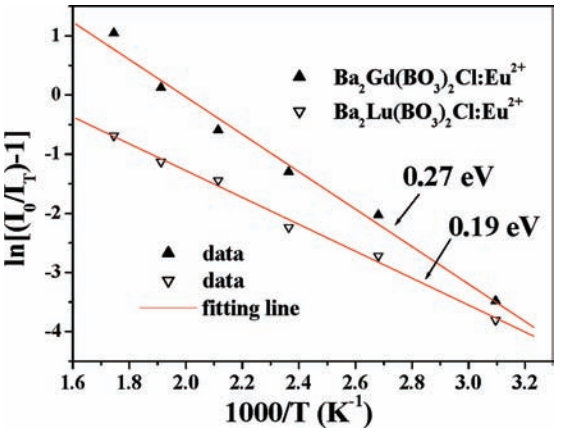

Figure 10. Activation energy for thermal quenching of $Ba_2Gd(BO_3)_2Cl:0.03Eu^{2+}$ and $Ba_2Lu(BO_3)_2Cl:0.03Eu^{2+n}$ phosphors.

to the different temperature dependence photoluminescence behavior originating from the two existing emission centers. First, we have excluded the influence of the temperature dependent structure by comparatively studying the phase structure of $Ba_2Y(BO_3)_2Cl$ at room temperature and after heat treatment of 200 °C, as given in Figure S4. No obvious difference in their XRD patterns can be found. Therefore, the increase of the emission intensity with increasing temperature should be ascribed to the difference of luminescence efficiency from the two emission centers, and the emission centers at the short wavelength side play the key role in this process, as also found for the blue-shift behavior. However, its detailed luminescence mechanism and process are intriguing enough to warrant further exploration in the future work.

$$I_T = \frac{I_0}{1 + c\exp\left(-\frac{\Delta E}{kT}\right)} \quad (5)$$

In order to understand the temperature dependence of emission intensity and to determine the activation energy for thermal quenching, the Arrhenius equation was fitted to the thermal quenching data of the $Ba_2Gd(BO_3)_2Cl:0.03Eu^{2+}$ and $Ba_2Lu(BO_3)_2Cl:0.03Eu^{2+}$ phosphors, as shown in Figure 10.[26,27] As demonstrated in eq 5, the probability of thermal activation is strongly dependent on the temperature, resulting in the decrease of emission intensity. In eq 5, I_0 is the initial emission intensity, I_T is the intensity at different temperatures, ΔE is activation energy of thermal quenching, c is a constant for a certain host, and k is the Boltzmann constant (8.629×10^{-5} eV). Figure 10 plots the relationship of $\ln[(I_0/I_T) - 1]$ versus $1000/T$ for the two kinds of phosphors, which is linear with a slope of −3.08 ($Ba_2Gd(BO_3)_2Cl:0.03Eu^{2+}$) and −2.27 ($Ba_2Lu(BO_3)_2Cl:0.03Eu^{2+}$). According to eq 5, the activation energy ΔE was calculated to be 0.27 and 0.19 eV, respectively. Usually, ΔE is related to the energy gap between the lowest energy $Eu^{2+}(4f^6 6s^0 5d^1)$ excited level and the bottom of the conduction band, which is connected with thermally activated energy transfer processes. Compared with the previous reports on the calculated activation energy corresponding to the thermally stable phosphors,[28] $Ba_2Gd(BO_3)_2Cl:0.03Eu^{2+}$ and $Ba_2Lu(BO_3)_2Cl:0.03Eu^{2+}$ phosphors have a high or comparable activation energy value.

dx.doi.org/10.1021/ic200988w |Inorg. Chem. 2011, 50, 10134–10142

4. CONCLUSIONS

In this work, we present a systematic study on the synthesis, structures analysis, and photoluminescence properties of a series of novel chloroborate phosphors $Ba_2Ln(BO_3)_2Cl:Eu^{2+}$ (Ln = Y, Gd and Lu), especially those phosphors showing thermally stable luminescent properties. The successful isomorphic substitution for Ln^{3+} sites in $Ba_2Ln(BO_3)_2Cl$ host by other trivalent rare earth ions, Sm, Eu, Tb, Dy, Ho, Er, Tm, Yb, has been found, and the crystal structures for $Ba_2Ln(BO_3)_2Cl$ (Ln = Y, Gd, and Lu) were refined by the Rietveld method. Under 365 UV light excitation, $Ba_2Ln(BO_3)_2Cl:Eu^{2+}$ phosphors exhibit bluish-green/greenish-yellow light with peak wavelengths at 526, 548, and 511 nm for $Ba_2Y(BO_3)_2Cl:Eu^{2+}$, $Ba_2Gd(BO_3)_2Cl:Eu^{2+}$, and $Ba_2Lu(BO_3)_2Cl:Eu^{2+}$, respectively. Furthermore, this series of $Ba_2Ln(BO_3)_2Cl:Eu^{2+}$ phosphors have high thermal quenching temperatures, and their emission bands show a blue-shift with broadening bandwidth. The more important and interesting phenomenon is that $Ba_2Y(BO_3)_2Cl:0.03Eu^{2+}$ phosphor has an abnormal temperature dependent emission property. The emission intensity increases from room temperature to 200 °C, and then decreases slightly. The present results suggest that our exploration in the novel chloroborate phosphor $Ba_2Ln(BO_3)_2Cl:Eu^{2+}$ are helpful for understanding the crystal structure and photoluminescence properties and developing new materials as the wavelength-conversion phosphors for use in white-light UV-LEDs.

■ ASSOCIATED CONTENT

Ⓢ Supporting Information. TG-DTA curves for the synthesis of $Ba_2Y(BO_3)_2Cl$. Bond data and the bond distances range for $Ba_2Ln(BO_3)_2Cl$ (Ln = Y, Gd, and Lu) compounds. Decay curves and corresponding fitting of $Ba_2Ln(BO_3)_2Cl:Eu^{2+}$ (Ln = Y, Gd, and Lu) phosphors. Temperature dependent PL spectra and XRD patterns of $Ba_2Y(BO_3)_2Cl:Eu^{2+}$ phosphors. This material is available free of charge via the Internet at http://pubs.acs.org.

■ AUTHOR INFORMATION

Corresponding Author

*E-mail: xiazg426@yahoo.com.cn. Phone: +86-10-8232-2759. Fax.: +86-10-8232-2974.

■ ACKNOWLEDGMENT

The authors gratefully acknowledge the National Natural Science Foundations of China (Grant 51002146), the Ph.D. Programs Foundation of Ministry of Education of China (Grant 20090022120002), the Fundamental Research Funds for the Central Universities (2010ZY35, 2011YXL005), and the Funds of the State Key Laboratory of Rare Earth Resource Utilization, Changchun Institute of Applied Chemistry, Chinese Academy of Sciences (RERU2011014).

■ REFERENCES

(1) (a) Izumi, H. K.; Kirsch, J. E.; Stern, C. L.; Poeppelmeier, K. R. *Inorg. Chem.* **2005**, *44*, 884. (b) Sauvage, F.; Bodenez, V.; Tarascon, J.-M.; Poeppelmeier, K. R. *Inorg. Chem.* **2010**, *49*, 6461. (c) Chamberlain, J. M.; Albrecht, T. A.; Lesage, J.; Sauvage, F.; Stern, C. L.; Poeppelmeier, K. R. *Cryst. Growth Des.* **2010**, *10*, 4868.

(2) (a) Wang, W. N.; Iskandar, F.; Okuyama, K.; Shinomiya, Y. *Adv. Mater.* **2008**, *20*, 3422. (b) Wang, W. N.; Kaihatsu, Y.; Iskandar, F.; Okuyama, K. *Chem. Mater.* **2009**, *21*, 4865.

(3) (a) Zhang, Q. H.; Wang, J.; Zhang, G. G.; Su, Q. *J. Mater. Chem.* **2009**, *19*, 7088. (b) Guo, C. F.; Luan, L.; Shi, L.; Seo, H. J. *Electrochem. Solid-State Lett.* **2010**, *13*, J28.

(4) (a) Akella, A.; Keszler, D. A. *Chem. Mater.* **1996**, *7*, 1299. (b) Liu, J.; Lian, H. Z.; Shi, C. S.; Sun, J. Y. *J. Electrochem. Soc.* **2005**, *152*, G880.

(5) (a) Setlur, A. A.; Radkov, E. V.; Henderson, C. S.; Her, J.-H.; Srivastava, A. M.; Karkada, N.; Kishore, M. S.; Kumar, N. P.; ; Aesram, D.; Deshpande, A.; Kolodin, B.; Grigorov, L. S.; Happek, U. *Chem. Mater.* **2010**, *22*, 4076. (b) Chen, W. P.; Liang, H. B.; Ni, H. Y.; He, P.; Su, Q. *J. Electrochem. Soc.* **2010**, *157*, J159.

(6) (a) Xie, M. B.; Tao, Y.; Huang, Y.; Liang, H. B.; Su, Q. *Inorg. Chem.* **2010**, *49*, 11317. (b) Song, Y. H.; You, H. P.; Yang, M.; Zheng, Y. H.; Liu, K.; Jia, G.; Huang, Y. J.; Zhang, L. H.; Zhang, H. J. *Inorg. Chem.* **2010**, *49*, 1674. (c) Tang, Y. S.; Hu, S. F.; Ke, W. C.; Lin, C. C.; Bagkar, N. C.; Liu, R. S. *Appl. Phys. Lett.* **2008**, *93*, 131114. (d) Chiu, Y. C.; Liu, W. R.; Chang, C. K.; Liao, C. C.; Yeh, Y. T.; Jang, S. M.; Chen, T. M. *J. Mater. Chem.* **2010**, *20*, 1755.

(7) (a) Xia, Z. G.; Sun, J. Y.; Du, H. Y.; Zhou, W. *Opt. Mater.* **2006**, *28*, 524. (b) Xia, Z. G.; Li, Q.; Sun, J. Y. *Mater. Lett.* **2007**, *61*, 1885.

(8) (a) Xia, Z. G.; Li, Q.; Sun, J. Y. *Chem. Lett.* **2006**, *35*, 764. (b) Xia, Z. G.; Liu, J.; Li, Q.; Sun, J. Y. *Electrochem. Solid-State Lett.* **2007**, *10*, J4. (c) Xia, Z. G.; Li, G. W.; Chen, D. M.; Xiao, H. Y. *Mater. Lett.* **2009**, *63*, 2600.

(9) Blasse, G.; Grabmaier, B. C. *Luminescent Materials*; Springer Verlag: Berlin, 1994.

(10) Meijerink, A.; Blasse, G. *J. Lumin.* **1990**, *47*, 1.

(11) (a) Nakamura, S.; Fasol, G. *The Blue Laser Diode: GaN Based Light Emitters and Lasers*; Springer: Berlin, 1997. (b) Zhang, S. Y.; Nakai, Y.; Tsuboi, Y.; Huang, Y. L.; Seo, H. J. *Inorg. Chem.* **2011**, *50*, 2897.

(12) Xia, Z. G.; Du, H. Y.; Sun, J. Y.; Chen, D. M.; Wang, X. F. *Mater. Chem. Phys.* **2010**, *119*, 7.

(13) Zhuang, J. Q.; Xia, Z. G.; Liu, H. K.; Zhang, Z. P.; Liao, L. B. *Appl. Surf. Sci.* **2011**, *257*, 4350.

(14) Xia, Z. G.; Li, Q.; Li, G. W.; Xiong, M.; Liao, L. B. *J. Cryst. Growth* **2011**, *318*, 958.

(15) *TOPAS V2.1, General Profile and Structure Analysis Software for Powder Diffraction Data*; Bruker AXS: Karlsruhe, Germany, 2003.

(16) Khamaganova, T. N.; Nevskii, N. N.; Trunov, V. K. *Sov. Phys. Cryst.* **1989**, *34*, 853.

(17) Schipper, W. J.; Blasse, G. *J. Alloys Compd.* **1994**, *203*, 267.

(18) Ferro, O.; Merlino, S.; Vinogradova, S. A.; Pushcharovsky, D. Y.; Dimitrova, O. V. *J. Alloys Compd.* **2000**, *305*, 63.

(19) Van Uitert, L. G. *J. Lumin.* **1984**, *29*, 1.

(20) Huang, C. H.; Chen, T. M.; Liu, W. R.; Chiu, Y. C.; Yeh, Y. T.; Jang, S. M. *ACS Appl. Mater. Interfaces* **2010**, *2*, 259.

(21) Shionoya, S.; Yen, W. M. *Phosphor Handbook*; CRC Press, New York, 1998.

(22) Varshini, Y. P. *Physica* **1967**, *34*, A149.

(23) Kim, J. S.; Park, Y. H.; Kim, S. M.; Choi, J. C.; Park, H. L. *Solid State Commun.* **2005**, *133*, 445.

(24) Qin, C. X.; Huang, Y. L.; Shi, L.; Chen, G. Q.; Qiao, X. B.; Seo, H. J. *J. Phys. D: Appl. Phys.* **2009**, *42*, 185105.

(25) Mikhailikm, V. B.; Kraus, H.; Wahl, D.; Itoh, M.; Koike, M.; Bailiff, I. K. *Phys. Rev. B* **2004**, *69*, 205110.

(26) Henderson, B.; Imbusch, G. F. *Optical Spectroscopy of Inorganic Solids*; Clarendon Press: Oxford, 1989.

(27) Chen, Y.; Liu, B.; Shi, C.; Ren, G.; Zimmerer, G. *Nucl. Instrum. Methods Phys. Res., Sect. A* **2005**, *537*, 31.

(28) (a) Xie, R.-J.; Hirosaki, N.; Kimura, N.; Sakuma, K.; Mitomo, M. *Appl. Phys. Lett.* **2007**, *90*, 191101. (b) Ryu, J. H.; Park, Y. G.; Won, H. S.; Kim, S. H.; Suzuki, H.; Lee, J. M.; Yoon, C.; Nazarov, M.; Noh, D. Y.; Tsukerblat, B. *J. Electrochem. Soc.* **2008**, *155*, J99. (c) Baginskiy, I.; Liu, R. S. *J. Electrochem. Soc.* **2009**, *156*, G29.